Spinning pipe gas lens aberrations along the axis and in the boundary layer

AUTHORS:
Cosmas Mafusire[1]
Andrew Forbes[1,2,3,4]

AFFILIATIONS:
[1]CSIR National Laser Centre, Pretoria, South Africa
[2]School of Physics, University of KwaZulu-Natal, Durban, South Africa
[3]School of Physics, Stellenbosch University, Stellenbosch, South Africa
[4]School of Physics, University of the Witwatersrand, Johannesburg, South Africa

CORRESPONDENCE TO:
Cosmas Mafusire

EMAIL:
cmafusire@csir.co.za

POSTAL ADDRESS:
CSIR National Laser Centre, PO Box 395, Pretoria 0001, South Africa

DATES:
Received: 28 Mar. 2013
Revised: 21 Jul. 2013
Accepted: 05 Aug. 2013

KEYWORDS:
gas lenses; graded index lenses; Shack-Hartmann sensor; optical aberrations; aerodynamic media

HOW TO CITE:
Mafusire C, Forbes A. Spinning pipe gas lens aberrations along the axis and in the boundary layer. S Afr J Sci. 2013;109(11/12), Art. #2013-0083, 6 pages. http://dx.doi.org/10.1590/sajs.2013/20130083

When the walls of an open-ended horizontal steel pipe are heated before the pipe is rotated along its axis, the exchange of the expelled heated air with the incoming cooler air, sucked in along the axis, results in a medium capable of focusing a laser beam propagating along the pipe's axis – a spinning pipe gas lens. However, the interaction of the heated and cooler air generates local density fluctuations which generate aberrations on the laser beam wavefront. We present results for the characterisation of these aberrations using a Shack-Hartmann wavefront sensor. The measurements show that along the axis, rotating the pipe decreases *y*-tilt as a result of the removal of distortions caused by gravity, although there is an increase in higher-order aberrations. However, in the boundary layer, the dominant aberration is *x*-astigmatism which increases with rotation speed. The results are confirmed by the measurement of the beam quality factor which increases as a result of the increase in the size of the higher-order aberrations. The spinning pipe gas lens is a device which can be used to focus laser beams using air only, but, in the process, the air introduces distortions which reduce the quality of the beam.

Introduction

We explored the aberrations generated by a heated spinning pipe – an open-ended steel pipe heated and rotated along its axis. It is well known that the resulting density distribution inside the pipe is conducive to focusing laser beams through the gradient index (GRIN) lens principle.[1-8] The spinning pipe gas lens was invented by Martynenko[1], and was subsequently developed for use as a 'damage-free' lens for focusing of high-power laser fields,[2-4] and as a gas telescope for astronomical imaging[6]. The principle of operation is simple: the shear viscosity of air increases when heated,[9] such that when the outside wall of the pipe is heated, the layer of air next to the pipe's inner wall is heated as well. During rotation, this inner layer is centrifugally expelled and replaced by cold air from the surroundings, inhaled along the axis from both ends, resulting in an axial (air) region that is cooler than the air at the wall. This temperature gradient results in a refractive index gradient that is conducive to focusing; thus the name, the spinning pipe gas lens (SPGL). The focal strength of the lens is a function of the physical dimensions of the pipe, and can be controlled through the rotation speed and wall temperature of the pipe.[7,8,10]

To fully understand how it operates, a computational fluid dynamics (CFD) model was prepared, based on the so-called k-ε model, to help illustrate the flow dynamics to establish the relationship among the rotation speed, temperature and the optical changes in the beam. The model was set at a wall temperature of 100 °C and a rotational speed of 20 Hz. It is apparent that, in terms of the rotation speed, the SPGL has two flow regimes: free convection in the stationary state, usually referred to as convective turbulence, and axisymmmetric forced convection during rotation; a CFD model of the two states is shown in Figure 1. In between the two flows, when the speed of rotation is neither too slow nor too fast, a combination of the two states exists, transitional between the two, which we refer to as mixed convection. It is also apparent that, during steady-state rotation, the SPGL has three main sections: the two ends where the hot and cold air exchange takes place and the centre where the gas flow is mainly circulatory. The gas from the environment is sucked from the surroundings from both ends along the axis and is heated up as it approaches the centre, replacing the warm air which is centrifuged out in a helical flow along the walls. The longitudinal speed of this incoming gas steadily decreases as its rotational speed increases. The centre of the pipe is dominated by rotational flow with little exchange with the environment, which results in the density distribution of the gas lens shown in Figure 2a, as calculated from the CFD model. In between the centre and the two ends, there exists transitional regions which are conducive to focusing, in which the cross-sectional density distribution is parabolic or even quartic, as shown by the cross-sections in Figure 2a. This is because the gradual transition from the cooler denser axis to the hot, less dense boundary layer creates a graded refractive index (GRIN) distribution in the transitional regions. The model also confirms that the two focusing regions are very short compared to the entire length of the SPGL. The centre steadily accumulates heat, making this part of the SPGL slightly hotter than the adjacent walls. This result can be explained by the CFD model which shows that the density at this centre is lower than that at the walls by an amount of 4×10^{-5} kg/m^3 (as illustrated in Figure 2b), translating to the centre being hotter by about 0.16 K. The temperature (T) distribution was extracted from the density (ρ) data using the relation $\rho = \rho_0 (1 - \alpha (T - T_0)$, where $\alpha = 2.263123 \times 10^{-4}$ K^{-1} is the coefficient volume expansion of air and ρ_0 is the known density at a known temperature, T_0. More detailed analysis of the SPGL CFD model is available in Mafusire and Forbes[10].

Propagation of an optical field through this medium results in cumulative phase variations, which distort the wavefront of the light by imparting aberrations onto the field. This phase can be characterised by a direct measurement of the wavefront of the light, the magnitude of the aberrations imparted, and the consequent deleterious effect on the laser beam quality factor.[11-13] We elected to decompose our wavefront using the Zernike polynomial set[14,15] whose first 11 polynomials are listed in Table 1. The optical aberrations, which are the weights of each polynomial in the decomposition, can individually or collectively be related to the beam quality factor (M^2)[11-13] and the wavefront error[16]. Potentially, the aberration composition can be used to estimate the focal length of the lens,[17] although we have not taken this approach in this paper. In this paper, we present results from aberration measurements generated by an SPGL on a HeNe laser beam transmitted through the SPGL's axis and boundary layer.

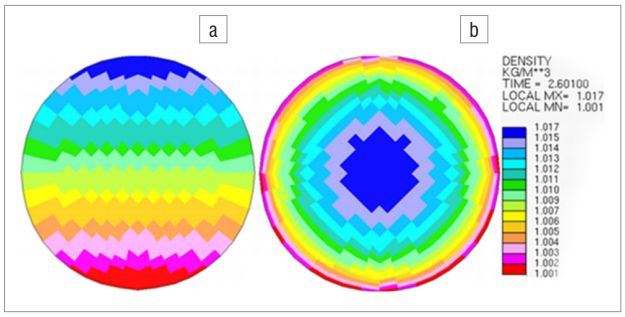

Figure 1: Cross-sectional density profiles of a spinning pipe gas lens showing (a) the initial state after heating and (b) the rotating steady-state near the end face of the pipe, with high density centre (blue) and low density edges (red).

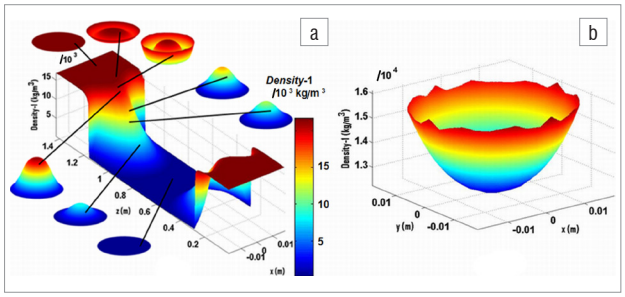

Figure 2: (a) A three-dimensional longitudinal density profile for the spinning pipe gas lens showing transverse sections at critical planes with two-dimensional profiles and (b) the transverse density profile at the centre of the spinning pipe gas lens.

Table 1: Zernike primary aberrations

n	*m*	Name of aberration and symbol	Polynomial
0	0	Piston, A_{00}	1
1	-1	*y*-Tilt, B_{11}	$\sqrt{2}\rho \sin \Theta$
	1	*x*-Tilt, A_{11}	$\sqrt{2}\rho \cos \Theta$
2	-2	*y*-Astigmatism, B_{22}	$\sqrt{6}\rho^2 \sin 2\Theta$
	0	Defocus, A_{20}	$\sqrt{3}(2\rho^2 - 1)$
	2	*x*-Astigmatism, A_{22}	$\sqrt{6}\rho^2 \cos 2\Theta$
3	-3	*y*-Triangular astigmatism, B_{33}	$\sqrt{8}\rho^3 \sin 3\Theta$
	-1	*y*-Primary coma, B_{31}	$\sqrt{6}(3\rho^3 - 2\rho) \sin \Theta$
	1	*x*-Primary coma, A_{31}	$\sqrt{8}(3\rho^3 - 2\rho) \cos \Theta$
	3	*x*-Triangular astigmatism, A_{33}	$\sqrt{8}\rho^3 \cos 3\Theta$
4	0	Spherical aberration, A_{40}	$\sqrt{5}(6\rho^4 - 6\rho^2 + 1)$

Experimental set-up

Two basic experiments were carried out. In the first experiment, the laser beam was propagated along the axis of the pipe, while in the second, the beam was propagated in the boundary layer (9.1 mm above the axis in this case) close to the pipe wall but taking care not to introduce unwanted distortions caused by hard edge diffraction of the beam. The situations are illustrated with a cross-section of the SPGL in Figure 3a. Our SPGL comprised a 1.43-m long stainless steel pipe with an internal diameter of 36.6 mm. The rotation was facilitated by two electric motors, one on each end of the pipe, with the rotating spindles on the motors attached to the pipe itself by rubber bands. The motors and pipe were independently attached to a metal stand to convert everything into a single device. The pipe was rotated along its axis with the aid of ball bearings located about 250 mm from each end. Rotation occurred as a result of a controlled voltage supply to the motors, which enabled a maximum rotation speed of just over 18 Hz. This device, the SPGL, was then fixed on an optical table on top of a rubber mat to absorb vibrations caused by the rotation. A picture of the SPGL is available as Figure 1 in Mafusire and Forbes[10]. Note that the pipe is of the same dimensions as the one used in the CFD model (Figure 2). The pipe was electrically heated using a resistive heater which was wound in the pipe's central 0.93-m section; the end sections of about 250 mm each, as determined by the location of the ball bearing mechanism, were not sealed with heating tape. Measurements of the temperatures along the pipe wall were taken by a series of thermocouples placed along the pipe length, from which a single value was acquired by calculating their average. The walls of the stationary pipe were heated to the required temperature and then the thermocouples were removed before rotation could commence. Copper brushes were used for electrical contact to ensure that the temperature of the pipe wall was maintained even during rotation of the pipe. The rotation speed was measured using an opto-switch circuit together with a cathode ray oscilloscope. For details of the opto-switch circuit design, please see Mafusire[18].

To measure the phase generated by the SPGL, a Shack-Hartmann wavefront sensor (model CLAS 2D with a 69x69 microlens grid of size 7.4 mm × 7.4 mm, WaveFront Sciences Inc., Albuquerque, NM, USA) was used to capture the wavefront of a HeNe laser beam after the beam had passed through the gas lens. The sensor was placed on a separate optical table to minimise the impact of the vibrations on the sensor. The laser beam was first expanded by a ×10 telescope to ensure a collimated laser beam passed through the axis of the pipe. A ×0.5 telescope custom made for this particular wavefront sensor was used to reduce the beam on exit from the pipe so that it could fit onto the wavefront sensor microlens grid. In the case of the boundary layer, the required beam size was acquired using a ×3.2 telescope and then measured on exit from the pipe without further adjustment. The resulting beam sizes ($1/e^2$ radius) in the two experiments were 10.6 mm and 3.4 mm inside the pipe along the axis and in the boundary layer, respectively, such that the Rayleigh length in both cases (~15 m and

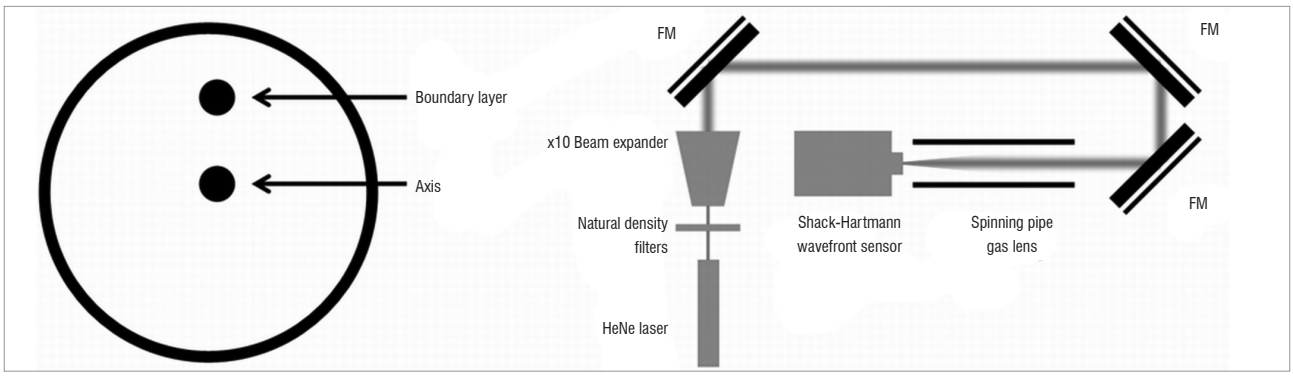

FM, flat mirror.

Figure 3: (a) A cross-section of the spinning pipe gas lens showing the propagation paths of laser beams along the axis and close to the wall above it. (b) Schematic of the experimental set-up for the measurement of the phase to determine turbulence parameters of the spinning pipe gas lens.

~8 m, respectively) was about an order of magnitude longer than the pipe length. Thus the beams could be considered collimated and free space propagation effects (such as wavefront curvature change) could be neglected. The complete experimental set-up is shown in Figure 3b.

The pipe wall temperature was varied between 21 °C and 155 °C at ~25-°C intervals. At each temperature, the rotation speed was varied from 0 Hz to ~20 Hz. A total of 36 parameter combinations were used to sample the space, with between 120 and 190 measurements taken at each to ensure adequate sampling for average and error analysis. The data were acquired at a rate of about 1 data point per second. The primary aberrations and the beam quality factor (M^2) were acquired simultaneously for each parameter combination. For each slope map, the average was calculated at each combination and subtracted from each map to give each one's deviation from the mean using a function built into the wavefront sensor software. The wall temperatures used were 21 °C, 53 °C, 77 °C, 103 °C, 126 °C and 155 °C, such that the wall differences, ΔT, were 0 K, 32 K, 56 K, 82 K, 105 K and 134 K with the ambient, which was set and maintained at 21 °C using the air-conditioning control fixture in the laboratory during measurement. The temperature was verified independently by direct measurement.

Experimental results

In order to fully understand flow in the gas lens, we present *rms* Zernike measurements of static aberrations of laser beams generated along the axis and in the boundary layer with the Zernike circle radius set at 7.28 mm (Figure 4). Here we have the wavefront errors of the primary aberrations for each of the rotation speeds for wall temperatures 77 °C, 103 °C, 126 °C and 155 °C, along the axis. As expected, the dominant aberration for a stationary heated pipe is the *y*-tilt (about 4 λ) because of the convective turbulence. As the rotation begins, it drops to almost zero, a result of the homogenisation which removes the impact of distortions caused by gravity. At the same time, the defocus aberration begins to increase with the increasing rotation speed, from a wavefront error of 0.2 λ^2 to 3 λ^2 at a wall temperature of 77 °C or 10 λ^2 at 155 °C. In general, higher defocus values are acquired for larger wall temperatures at a given rotation speed.

The results of the *rms* Zernike aberration measurements in the boundary layer are different from those in the axis, indicating the difference in the flow (Figure 5). With all temperatures, the aberrations reach a minimum at 2.95 Hz when the natural and forced convection are present in the pipe, then begin to rise again. We note also that the rotationally non-symmetric aberrations are dominating in this case. The dominant aberration is *x*-astigmatism (A_{22}) and is especially dominant at lower temperatures for the same rotation speed, stretching out the phase map. We also notice that for high rotation speed, at 126 °C and 155 °C, *y*-astigmatism (B_{22}) also begins to increase until it almost matches *x*-astigmatism as *x*-tilt increases sharply at 14.3 Hz and 18.1 Hz. It is these three aberrations which are primarily responsible for distortion in the phase.

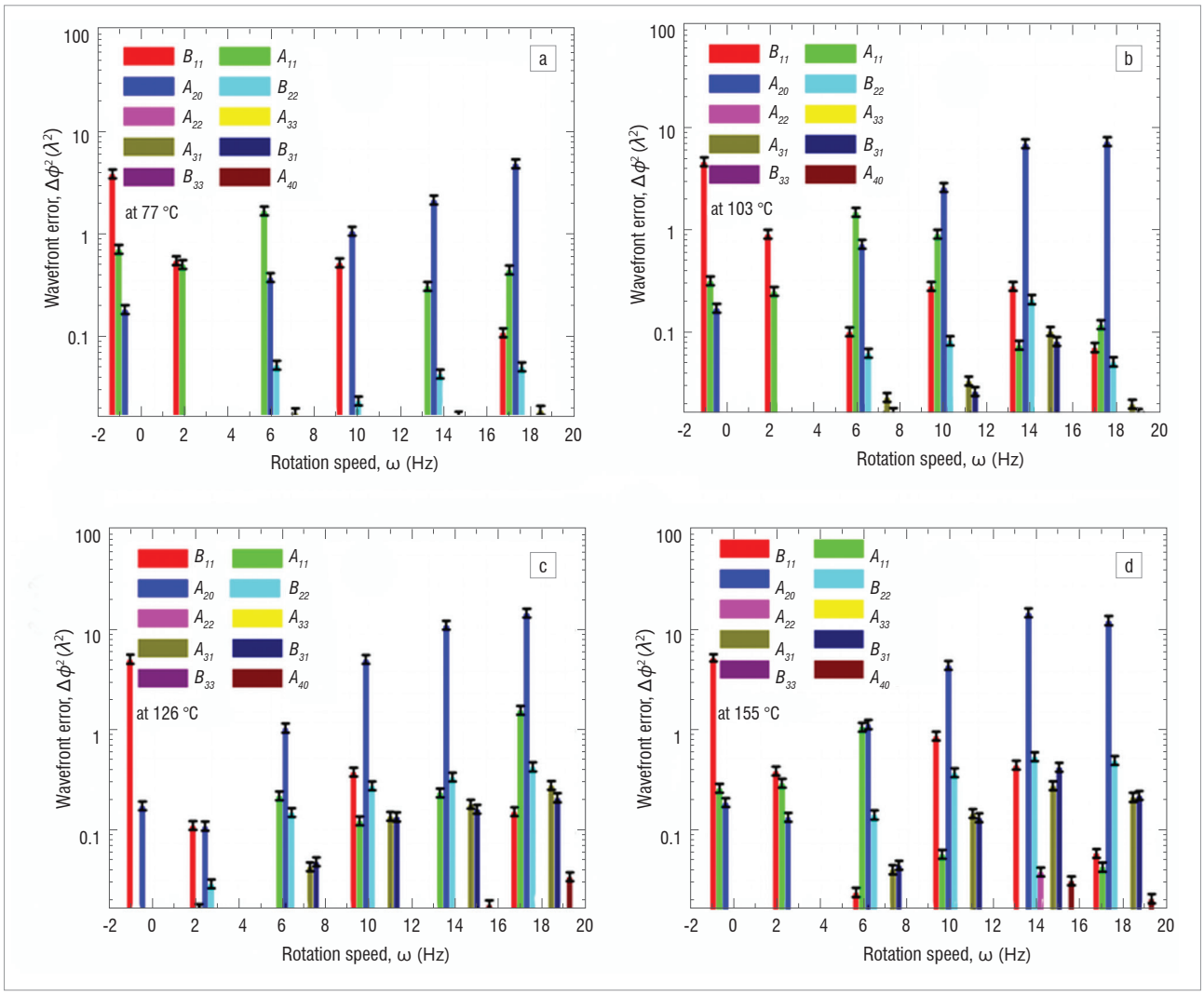

Figure 4: Wavefront error of primary aberration in the spinning pipe gas lens axis at rotation speeds 0 Hz, 2.95 Hz, 6.73 Hz, 10.5 Hz, 14.3 Hz and 18.1 Hz for selected wall temperatures. The Zernike radius was set at 7.28 mm.

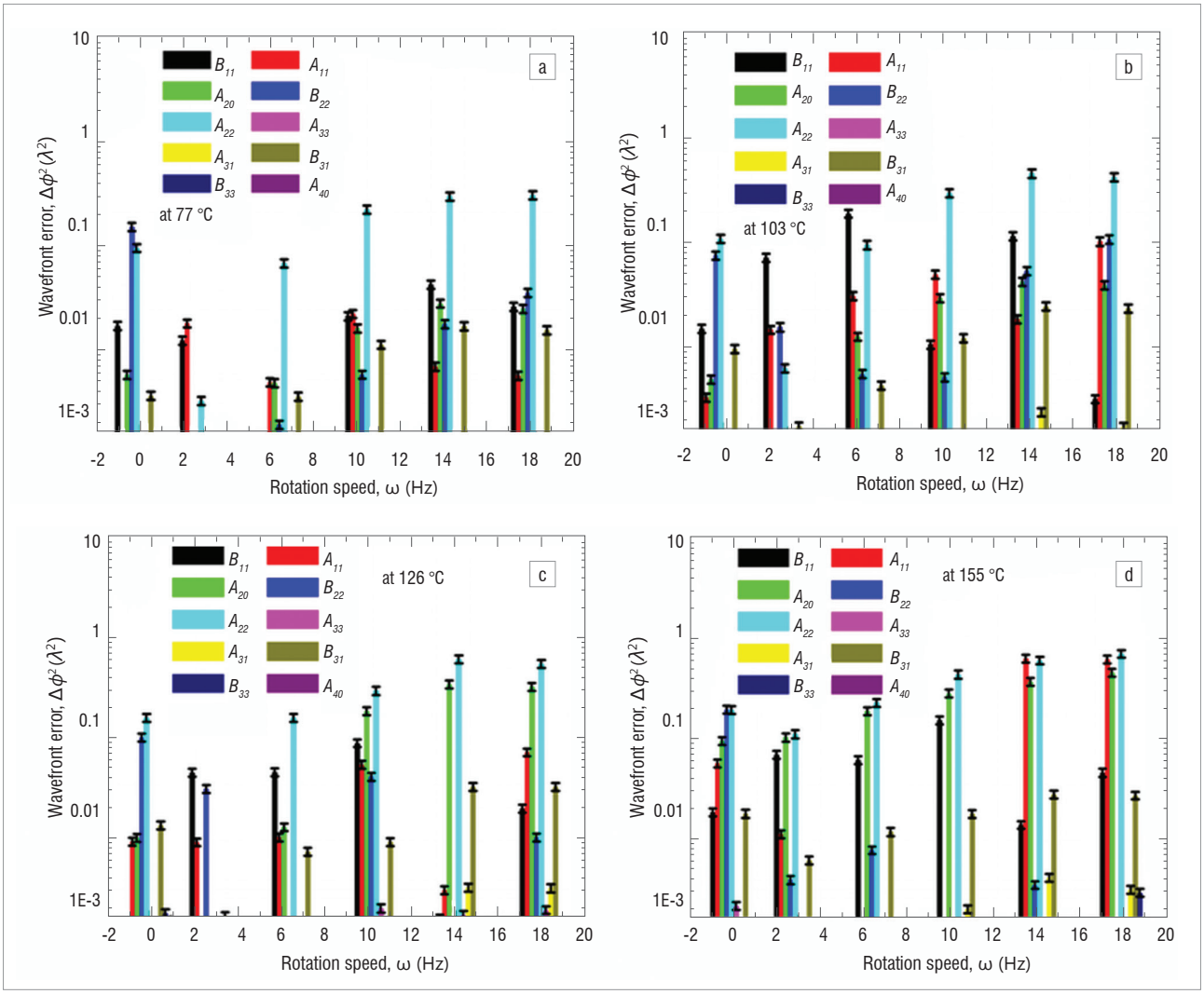

Figure 5: Wavefront error of primary aberration in the spinning pipe gas lens boundary layer at rotation speeds 0 Hz, 2.95 Hz, 6.73 Hz, 10.5 Hz, 14.3 Hz and 18.1 Hz for selected wall temperatures. The Zernike radius was set at 3.71 mm.

The average phase maps for the 120–190 frames for each data point determined by each of the selected input parameters are shown in Figure 6, with values on the left for axial propagation and those on the right for the boundary layer. Along the axis, there is a clear distinction among the three flow regimes – the natural, the mixed, and then the forced convections. The blue part of the phase indicates less of a phase delay than the red part. The natural convection is shown in the small top left-hand corner of the grid, the forced convection in the larger bottom right-hand corner and the mixed convection stretches diagonally in-between (Figure 6a). Under natural convection, the beam is slightly diverging with a fair amount of tilt as the centre of the phase patterns is located slightly lower than the centre of the aperture. At the onset of forced convection, the phase is dominated by negative defocus as the laser beam is focused with the tilt totally removed, especially at the highest rotation speed and wall temperature. The transition between the two convection states also occurs at lower rotation speeds and lower temperatures as the wall temperature increases. In the boundary layer there is a density gradient because of the GRIN effect, which tilts the beam as either rotation speed or temperature increase (Figure 6b). At 53 °C, rotating the pipe results in a significant temperature difference, which causes gas exchange with the environment and creates density variations, and so phase changes to the beam wavefront. The phase map, in fact, begins to stretch out, losing rotational symmetry. This asymmetry becomes observable at 10.5 Hz. At higher wall temperatures, the effect becomes observable at lower rotation speeds. At the highest rotation speeds, at all temperatures, we begin to notice that the phase pattern is being both stretched and tilted, losing symmetry along both *x*- and *y*-axes.

Taking a closer look at *x*- and *y*-astigmatism coefficients in the boundary layer, we see that A_{22} and B_{22} are always positive and negative, respectively, and almost symmetric about the horizontal axis (Figure 7) for the same temperature. Their magnitudes increase with increasing temperature. The magnitudes for the aberrations drop slightly as the rotation begins (2.95 Hz) and then begin to rise after that. The beam quality factor (M^2) seems to confirm this drop. We observe that the beam quality factor drops slightly at 2.95 Hz and rises at higher rotation speeds and increases with increasing rotation speed (Figure 8). This relation is true for M^2_x and M^2_y at all temperatures. We also see that the *y*-value is greater than the corresponding *x*-value at the same temperature. This difference is because the beam is diverging more slowly in the horizontal plane because of the phase gradient which increases with the increase in the power of the lens.

Conclusions

This study continues earlier work in which the SPGL was revisited,[7,8] incorporating the full laser beam propagation through the system and the resulting wavefront changes. As stated previously, Martynenko[1] demonstrated the theoretical basis of the device which was later demonstrated as a possible practical tool for focusing high-power laser beams.[2-4] Using the device as a telescope objective[6] showed that the SPGL is an imperfect lens because the images produced

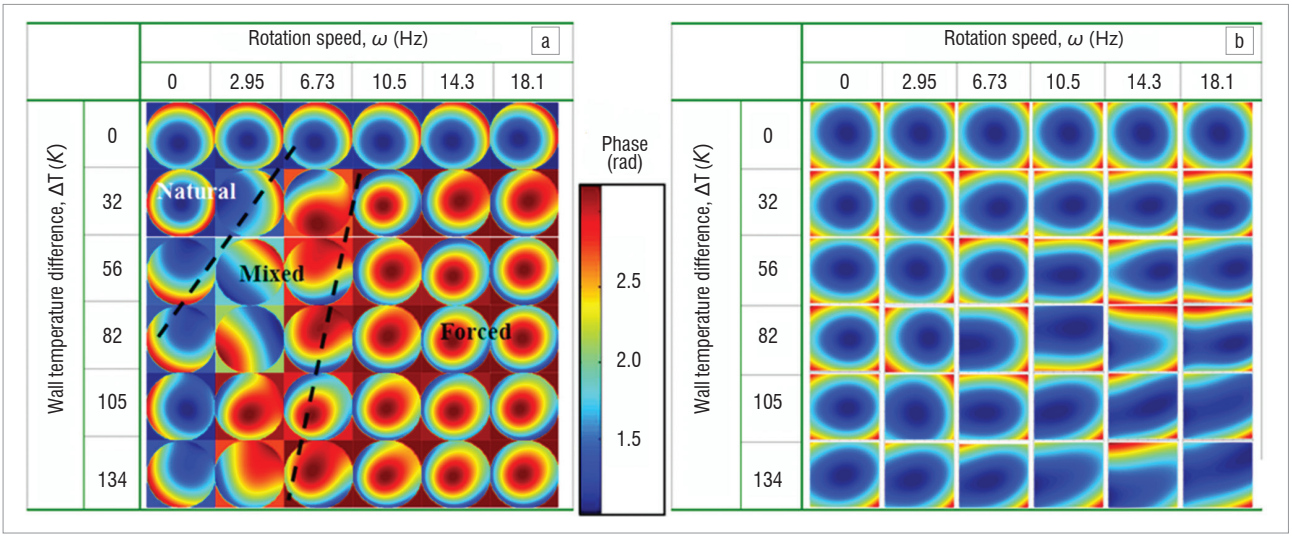

Figure 6: Average phase maps produced by the spinning pipe gas lens (a) axis and (b) boundary layer. The images on the left are apertured because these were focused beams. The images on the right were not apertured to show the effect of tilt on the phase.

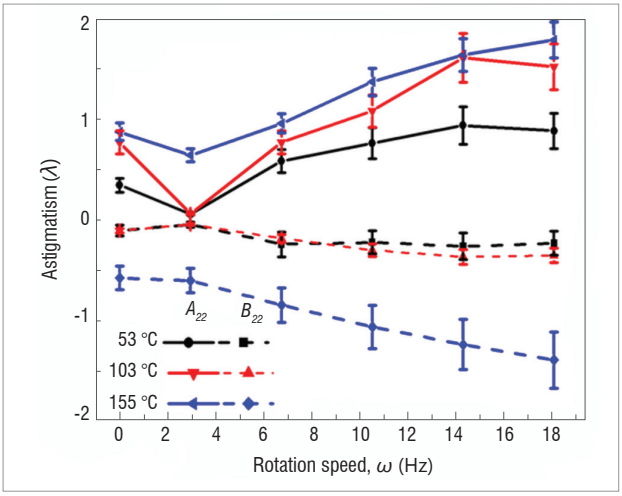

Figure 7: *x*- and *y*-Astigmatism in the boundary layer of the spinning pipe gas lens at selected wall temperatures.

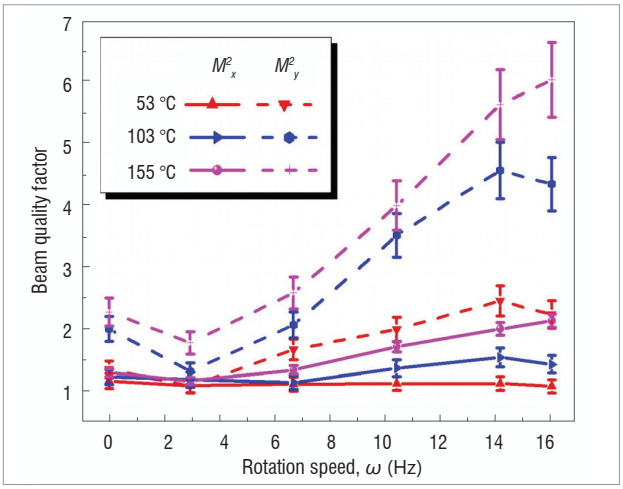

Figure 8: Boundary layer beam quality factor of the laser beam at selected wall temperatures.

were of low resolution, which we assume was a result of the large number of aberrations generated by the SPGL. This finding inspired us to characterise these aberrations using a CFD model[7,8,10] and direct measurement[7,8]. The CFD numerical model showed that the ends of the pipe contribute significantly to the overall focusing.[10] Direct measurement of the phase with a Shack-Hartmann sensor, as well as the focal length, were in agreement with the calculation from the model.[8]

We investigated the aberrations in the boundary layer in addition to the axial measurements for comparison. We have shown that rotating the SPGL along its axis removes distortions caused by natural convection as a result of gravity, because, at the onset of rotation, *y*-tilt aberration drops from 4 λ to almost 0. On the other hand, the defocus aberration increases with increasing rotation speed and wall temperature, i.e. as the lens gets stronger. This finding confirms our previous results.[7,8] In the boundary layer, the dominant aberrations are *x*- and *y*-astigmatism, which increase under the same conditions. The impact of *y*-tilt becomes very high in this part of the pipe during rotation, indicating the density gradient between the heated walls and the cooler axis, a condition which becomes more pronounced as the wall temperature and/or rotation speed increase.

The loss of beam quality as rotation speed and temperature increase is a result of the increase of the mixing of cooler incoming axial air with the warmer air next to the walls, which introduces density fluctuations, which in turn generate phase fluctuations in the laser beam wavefront, reducing the quality of the beam. This property can be used to turn the SPGL into a turbulence generator if the pipe turbulence can be properly characterised, and is the subject of future research efforts. For the moment, it is apparent that the SPGL represents a conundrum in that the operating conditions which make the lens stronger, that is higher wall temperature and greater rotation speed, also result in stronger turbulence being generated. A simultaneous general increase in all aberrations, both along the axis and in the boundary layers except *y*-tilt along the axis, is also observed, thereby reducing the quality of the beam. Therefore we believe it is best to use the device as a cheap, damage-free lens for focusing high-power laser beams, especially in cases where good beam quality might not be a pertinent issue. The behaviour of the lens in the boundary layer (Figure 6) shows that there is marginal focusing, achieving a maximum *rms* wavefront error of about 0.1 λ^2 in an aperture of radius 3.71 mm (or a focal length of 9.9 m) compared to a maximum *rms* wavefront error of 10 λ^2 in an aperture of radius 7.32 mm (or a focal length of 3.8 m) along the axis. We can therefore infer that the size of the beam should be no bigger than the effective aperture of the lens, which,

in this case, is of the order of 7.3 mm in radius about the axis (about 16% of the cross-sectional area). Enlarging the beam would most likely result in a reduction in the focusing power of the lens, and at the same time increase the amount of wavefront distortion.

Acknowledgements

We acknowledge Glenn Snedden of CSIR Defence, Peace, Safety and Security for creating the computational fluid dynamics model of the spinning pipe gas lens.

Authors' contributions

Both authors designed the experiment; C.M. performed the experiments and calculations; and A.F. was the project leader.

References

1. Martynenko OG. Aerothermooptics. Int J Heat Mass Transfer. 1975;18:793–796. http://dx.doi.org/10.1016/0017-9310(75)90208-2
2. Michaelis MM, Notcutt N, Cunningham PF. Drilling by a gas lens focused laser. Opt Comm. 1986;59:369–374. http://dx.doi.org/10.1016/0030-4018(86)90360-3
3. Michaelis MM, Notcutt M, Cunningham PF, Waltham JA. Spinning pipe gas lens. Opt Las Tech. 1988;20(5):243–250. http://dx.doi.org/10.1016/0030-3992(88)90025-4
4. Michaelis MM, Kuppen M, Forbes A, Viranna N, Lisi N. Progress with gas lenses. Laser Part Beams. 1996;14:473–485. http://dx.doi.org/10.1017/S0263034600010156
5. Lisi N, Bucellato R, Michaelis MM. Optical quality and temperature profile of a spinning pipe gas lens. Opt Las Tech. 1994;26:25–27. http://dx.doi.org/10.1016/0030-3992(94)90007-8
6. Michaelis MM, Dempers CA, Kosch AM, Prause A, Notcutt M, Cunningham PF, Waltham J. A gas lens telescope. Nature. 1991;353:547–548. http://dx.doi.org/10.1038/353547a0
7. Mafusire C, Forbes A, Michaelis MM, Snedden G. Optical aberrations in a spinning pipe gas gens. Opt Exp. 2008;16(13):9850–9856. http://dx.doi.org/10.1364/OE.16.009850
8. Mafusire C, Forbes A., Michaelis MM, Snedden G. Spinning pipe gas lens revisited. S Afr J Sci. 2008;104:260–264. http://dx.doi.org/10.1364/JOSAA.28.001372
9. Landau LD, Lifschitz EM. Fluid mechanics. 2nd ed. Oxford: Pergamon Books; 1987. p. 44–94.
10. Mafusire C, Forbes A. Aero-optics: Controlling light with air. In: Juarez LH, editor. Fluid dynamics. Computational modelling and applications [book on the Internet]. Rijeka: InTech; 2012. pp. 631–650. Available from: http://www.intechopen.com/books/fluid-dynamics- computational-modeling-and-applications/aero-optics-controlling-light-with-air
11. Mafusire C, Forbes A. The beam quality factor of truncated aberrated Gaussian laser beams. J Opt Soc Am A. 2011;28(7):1372–1378.
12. Alda J. Characterization of abberated laser beams. J Opt Soc Am A. 1997;14(10):2737–2747. http://dx.doi.org/10.1364/JOSAA.14.002737
13. Qiu Y, Gong M, Huang L, Liu Q, Yan P, Zhang H, et al. The beam quality of a truncated Gaussian beam with aberrations. Laser Phys Lett. 2013:10:055001. http://dx.doi.org/10.1088/1612-2011/10/5/055001
14. Born M, Wolf E. Principles of optics: Electromagnetic theory of propagation, interference and diffraction of light. 7th ed. Cambridge: Cambridge University Press; 1998. p. 517–553.
15. Mahajan VN. Optical imaging and aberration. Part 1: Ray geometrical optics. Bellingham, WA: SPIE Press; 1998. http://dx.doi.org/10.1117/3.265735
16. Mahajan VN. Strehl ratio of a Gaussian beam. J Opt Soc Am A. 2005;22(9):1824–1833.
17. Mafusire C, Forbes A. The mean focal length of an aberrated lens. J Opt Soc Am A. 2011;28(7):1403–1409. http://dx.doi.org/10.1364/JOSAA.28.001403
18. Mafusire C. Gas lensing in a heated rotating pipe [MSc thesis]. Harare: University of Zimbabwe; 2006.